

**Structural studies of human TFIID reveal a dramatic structural rearrangement
upon binding to core promoter DNA**

by

Michael A. Cianfrocco

A dissertation submitted in partial satisfaction of the

requirements for the degree of

Doctor of Philosophy

in

Biophysics

in the

Graduate Division

of the

University of California, Berkeley

Committee in charge:

Professor Eva Nogales, Chair

Professor James Berger

Professor Robert Glaeser

Professor Michael Levine

Fall 2012

The dissertation of Michael A. Cianfrocco, titled Structural studies of human TFIID reveal a dramatic structural rearrangement upon binding to core promoter DNA, is approved:

Chair _____

Date _____

Date _____

Date _____

Date _____

University of California, Berkeley

**Structural studies of human TFIID reveal a dramatic structural rearrangement
upon binding to core promoter DNA**

Copyright 2012
by
Michael A. Cianfrocco

Abstract

Structural studies of human TFIID reveal a dramatic structural rearrangement upon binding to core promoter DNA

by

Michael A. Cianfrocco

Doctor of Philosophy in Biophysics

University of California, Berkeley

Professor Eva Nogales, Chair

A mechanistic description of metazoan transcription is essential for understanding the molecular processes that govern cellular decisions. To provide structural insights into the DNA recognition step of transcription initiation, we used single particle electron microscopy to visualize human TFIID with promoter DNA. This analysis revealed that TFIID co-exists in two predominant and distinct structural states that differ by a 100 translocation of TFIIDs lobe A. The transition between these structural states is modulated by TFIIA, as the presence of TFIIA and promoter DNA facilitates the formation of a novel rearranged state of TFIID capable of promoter recognition and binding. DNA-labeling and footprinting, together with cryo-EM studies, mapped the locations of the TATA, Inr, MTE, and DPE promoter motifs within the TFIID-TFIIA-DNA structure. The existence of two structurally and functionally distinct forms of TFIID suggests that the different conformers may serve as specific targets for the action of regulatory factors.

Dedication stuff.

Contents

Contents	ii
List of Figures	iii
1 Biochemical and structural support for a general model of promoter binding by TFIID	1
1.1 Detailed footprinting of TFIID-TFIIA-SCP	3
1.2 TFIID interacts with diverse promoter architectures through the rearranged conformation	6
1.3 DNA binding within the canonical conformation	9
1.4 TFIID-TFIIA-TFIIB-SCP adopts the rearranged conformation on promoter DNA	13
1.5 A general model of regulated DNA binding by TFIID	19
2 Conclusions and outlook	24
A methods	25

List of Figures

1.1	TFIID exhibits TFIIA-independent and TFIIA-dependent interactions with SCP DNA	2
1.2	Line profiles for DNase I footprinting gels of TFIID-SCP and TFIID-TFIIA-SCP	4
1.3	Structural model of DNase I and MPE-Fe footprinting results within the ternary TFIID-TFIIA-SCP(-66) complex	5
1.4	Core promoter architecture dictates TFIIA-dependent and TFIIA-independent interactions of TFIID with core promoter DNA	7
1.5	Line profiles for DNase I footprinting on mTATA promoter	8
1.6	TFIID-TFIIA interacts with SCP(mTATA) within the rearranged conformation	10
1.7	Lobe C interacts with promoter DNA within the canonical conformation in a similar manner as the rearranged state	12
1.8	Cryo-EM of TFIID-TFIIA-TFIIB-SCP(-66)	14
1.9	TFIIB interacts with TFIID-TFIIA-SCP within the rearranged conformation on promoter DNA	15
1.10	TFIIB does not induce strong TATA box protection within TFIID-TFIIA-TFIIB-SCP(mTATA)	16
1.11	3D reconstruction of the rearranged conformation of TFIID-TFIIA-TFIIB-SCP(-66) reveals similar topology as TFIID-TFIIA-SCP(-66)	18
1.12	Model for SCP DNA binding by TFIID-TFIIA	20
1.13	Model for SCP(mTATA) DNA binding by TFIID-TFIIA	21
1.14	Model for SCP(mMTE/DPE) DNA binding by TFIID-TFIIA	22
1.15	TFIID may facilitate transcription initiation through topological changes in promoter DNA	23

Acknowledgments

Acknowledgement stuff.

Chapter 1

Biochemical and structural support for a general model of promoter binding by TFIID

The structural studies presented in Chapters 2 & 3 have provided the foundation for understanding the nature of TFIID's interaction with promoter DNA. However, in order to arrive at a more complete description of TFIID bound to promoter DNA, biochemical and structural studies were pursued in an attempt to propose a model of TFIID-TFIIA-SCP complex formation. To facilitate the biochemical studies, we engaged in a wonderful collaboration with James T. Kadonaga's laboratory at University of California - San Diego, where George A. Kassavetis performed all footprinting experiments shown in this chapter. The synergy between structural studies of TFIID-TFIIA-SCP and biochemical footprinting have helped construct the first model of human TFIID's regulated-interaction with promoter DNA.

This chapter will address potential mechanisms of promoter binding by TFIID through a variety of experimental designs. First, detailed footprinting analysis using DNase I and methidium-propyl-EDTA-Fe(II) reveal the extent of contacts that TFIID makes with promoter DNA in a TFIIA-dependent and -independent fashion. These footprinting results will be extended by testing the structural effect that core promoter mutations have on TFIID's structure. After developing a detailed model of TFIID-TFIIA-DNA, the canonical conformation will be probed to investigate the DNA binding activity, if any, that this conformation exhibits. Finally, cryo-EM structural analysis and footprinting will establish that the rearranged conformation is the TFIIB-binding conformation of TFIID, suggesting that the rearranged state is the conformation that loads RNAPII at the TSS. These results have been synthesized to propose a model that addresses the interplay between TFIID's conformational landscape and DNA binding (Figure 1.12)

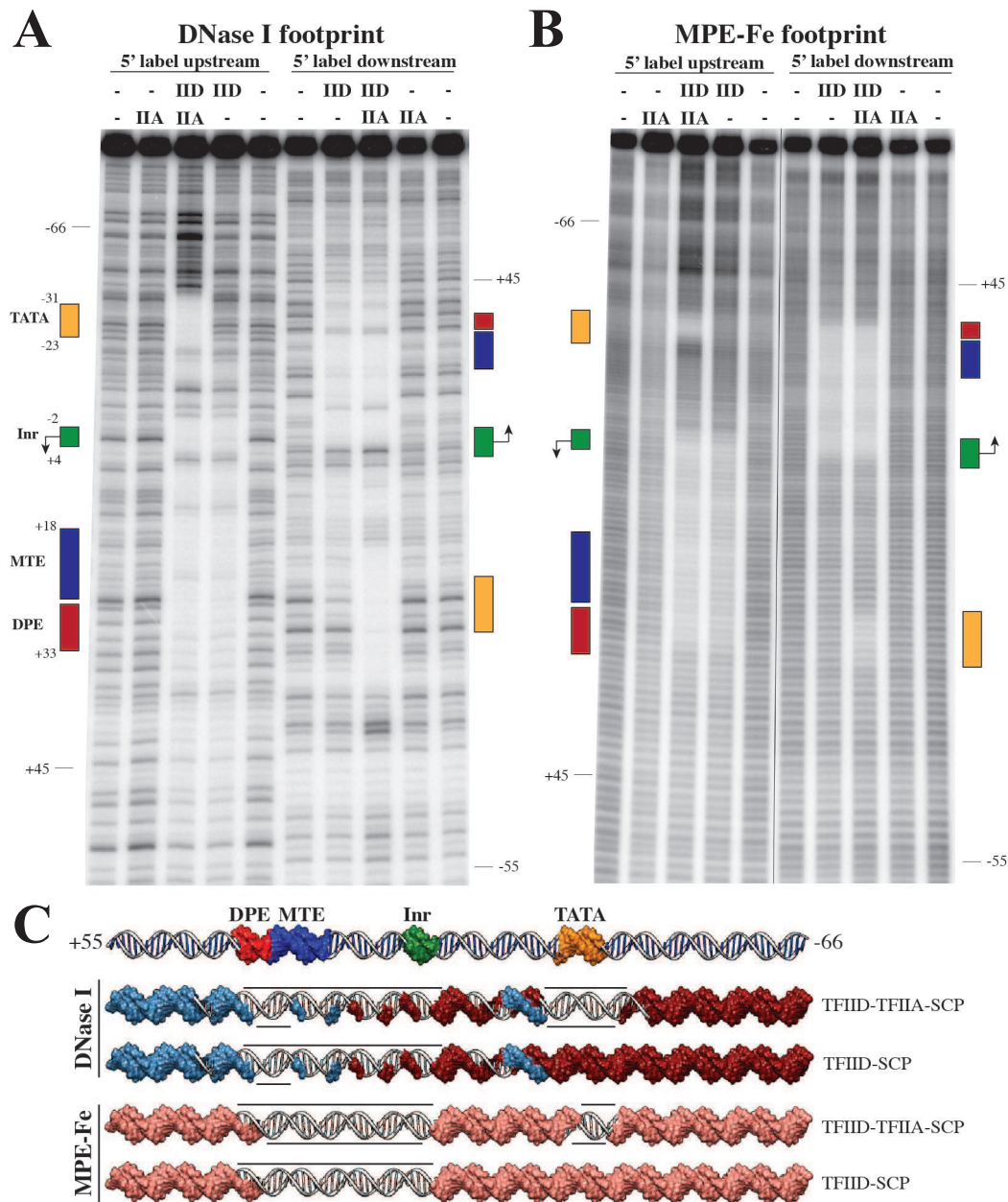


Figure 1.1: TFIID exhibits TFIIA-independent and TFIIA-dependent interactions with SCP DNA. DNase I (A) and MPE-Fe (B) footprinting of TFIID-SCP and TFIID-IIA-SCP. (C) B-DNA model of the SCP with positions of core promoter elements (top), DNase I, and MPE-Fe protection patterns (-66 to +55 shown) color-coded for TFIID-SCP and TFIID-IIA-SCP (four bottom rows). White basepairs indicate protection (also marked by black lines), blue surfaces indicate partial digestion and red surfaces indicate complete digestion by DNase I, and pink indicates digestion by MPE-Fe.

1.1 Detailed footprinting of TFIID-TFIIA-SCP

The cryo-EM data of the rearranged conformation of the TFIID-TFIIA-SCP complex suggest that the downstream DNA core promoter elements MTE and DPE are bound by lobe C, whereas the TATA box and possibly the Inr are bound by lobe A. To test and extend this model, we performed footprinting analyses of the TFIID-SCP complex in the presence or absence of TFIIA.

DNase I footprinting of TFIID-SCP showed an extended region of protection from -7 to +41, which is in agreement with previous footprinting data on TFIID-SCP (Figure 1.1A) [4]. The addition of TFIIA did not alter the downstream interactions of TFIID with the Inr, MTE, and DPE core promoter elements, but did, however, result in a substantial increase in the binding of TFIID to the TATA box and flanking DNA sequences from -38 to -20 (Figures 1.1A & 1.2A & B). DNase I footprinting analysis of both DNA strands in the absence or presence of TFIIA revealed distinct patterns of protection and cleavage throughout the core promoter region. The results indicate that the DNA sequence between the Inr and MTE/DPE sites exhibits a phasing in DNase I sensitivity in which one face of the SCP DNA between Inr and MTE-DPE is susceptible to DNase I cleavage, whereas the opposite face remains protected (Figure 1.1C). Furthermore, the accessible face of the DNA exhibits DNase I hypersensitivity upon binding of TFIID (Figure 1.1A).

To obtain high resolution data on the interactions of TFIID with the core promoter, we carried out footprinting analyses with methidiumpropyl-EDTA-Fe(II) (MPE-Fe), an intercalating agent that delivers Fe(II) for oxidation of the deoxyribose phosphate backbone of DNA and provides single bp resolution of protein-DNA contacts [3, 9, 14]. The MPE-Fe footprinting data on TFIID-SCP and TFIID-TFIIA-SCP revealed the extensive and continuous interaction of TFIID with DNA from the DPE through the Inr as well as the TFIIA-dependent protection of 8 bp (-31 to -24) of DNA encompassing the TATA box (Figures 1.1B & 1.2C & D). The strong stimulation of TFIID binding to the TATA box is consistent with the results of previous studies on the binding of TBP to DNA [2, 7, 6, 8]. The region of DNase I protection observed on only one face of the helix between the MTE/DPE and Inr also shows continuous protection from MPE-Fe(II) cleavage on both DNA strands, which is likely due to the inhibition of the DNA unwinding, necessary for MPE intercalation, that would occur as a result of protein bound to one side of the helix [13]. Thus, the DNase I and MPE-Fe footprinting results, summarized in Figure 1.1C, provide insight into the TFIID-DNA contacts that complements the cryo-EM data and contributes to the placement of the core promoter DNA on the TFIID structure.

The footprinting data provide new structural insight into the model of DNA through TFIID-TFIIA-SCP. Incorporating these footprinting data into the model reveals that the phasing of DNase I sensitive sites. On each strand between the Inr and MTE, there is a distinct 10 bp phasing of DNase I hypersensitive sites at -2, +18, and +28 (with probe DNA 5-labeled upstream) and at +4 and +13 (with probe DNA 5-labeled downstream) (Figure 1.1A). Incorporating this information into the cryo-EM model of TFIID-TFIIA-SCP allows for one side of the DNA sequence to face away from the central cavity (DNase I

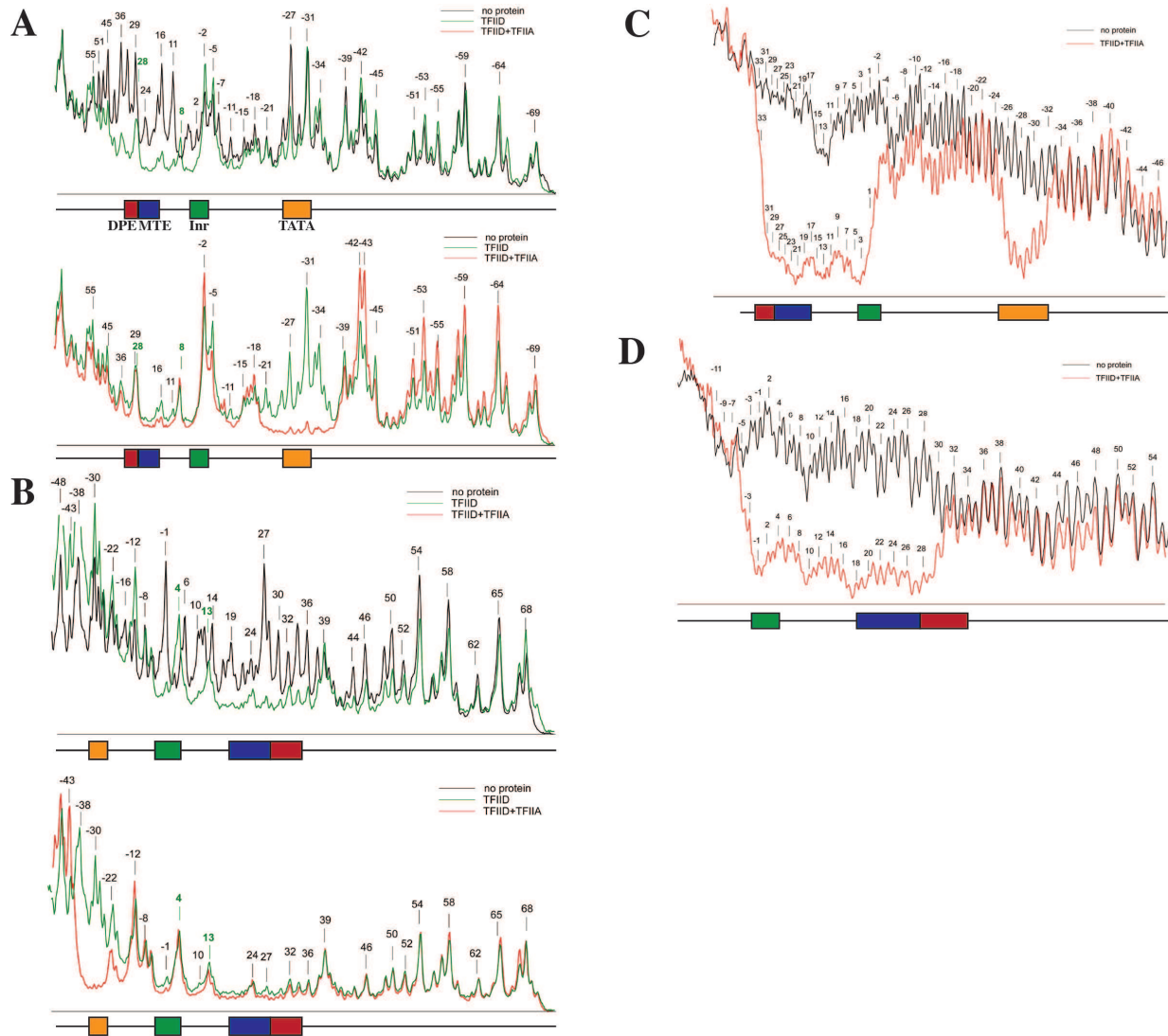


Figure 1.2: Line profiles for DNase I footprinting gels of TFIID-SCP and TFIID-TFIIA-SCP. (A) Line profile traces from DNase I footprinting gels for 5-label upstream (A) and downstream (B). Bold basepair numbers indicate hypersensitive sites. Line profile traces from MPE-Fe footprinting gels for 5-label upstream (C) and 5-label downstream (D).

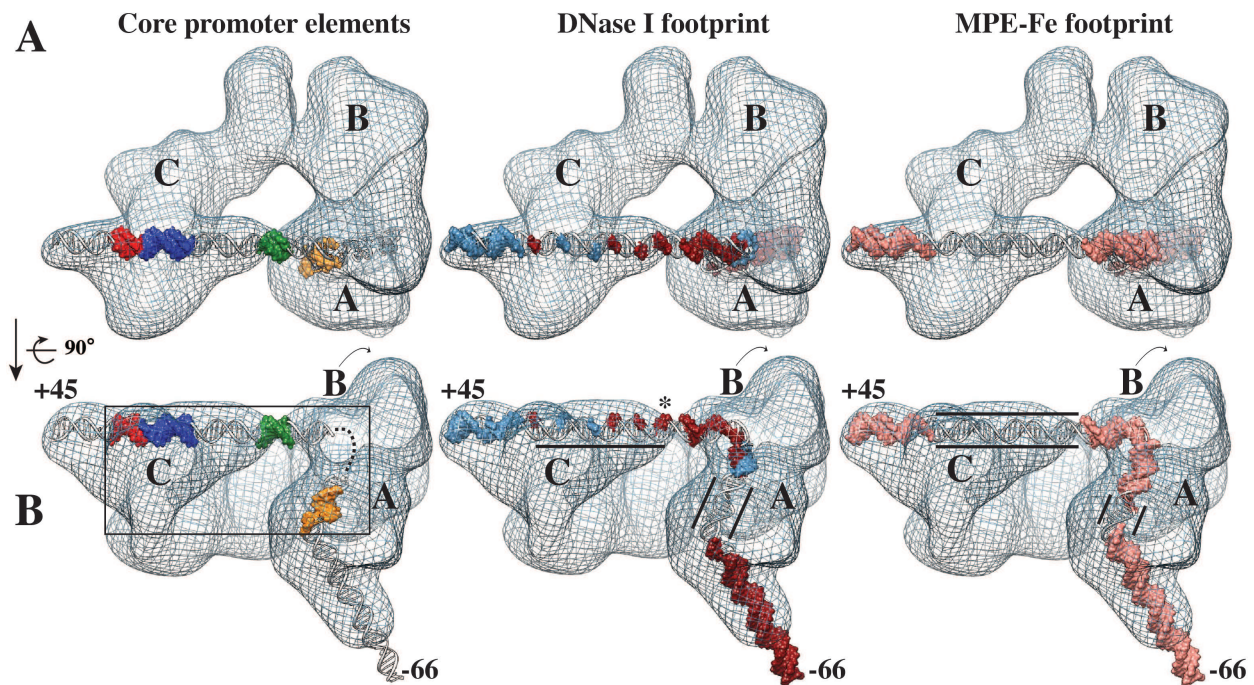


Figure 1.3: Structural model of DNase I and MPE-Fe footprinting results within the ternary TFIID-TFIIA-SCP(-66) complex. Promoter DNA for SCP(-66) docked into the TFIID-TFIIA-SCP(-66) map (shown in mesh). DNA models were taken from Figure 1.1 for sequences from -66 to +45. Asterisk in (B) indicates DNase I hypersensitive site at +3. Black lines in (B) indicate regions of continuous protection along SCP helix.

sensitive sites) while the opposite side of the helix faces the inner cavity of TFIID (DNase I protected sites) (Figure 1.3). Hence, these data suggest that TFIID presents the DNase I-accessible face of this region of the core promoter to the bulk solution for interactions with RNAPII and other factors involved in transcription initiation.

As the DNA extends across the central channel and enter into lobe A, the footprinting data suggest that there are topological changes in the promoter DNA surrounding the TSS. For instance, the DNase I footprinting experiment shows a hypersensitive site at +3, indicating that the DNA has changed conformed for optimal cleavage by Dnase I only when bound to TFIID (Figures 1.1A). Given that the strength of this hypersensitive site appears to correlate with the strength of transcription initiation from a given promoter, it is interesting that this site is exposed within the central channel of TFIID, suggesting that TFIID-induced topological changes of DNA within the central channel are relevant for later steps in transcription initiation.

The modeled path of promoter DNA through TFIID-TFIIA-SCP suggested that, in addition to the kinking of the TATA box by TBP, there is an additional bend in promoter DNA (Figure 1.3)). To test this model, MPE-Fe footprinting revealed that the intervening DNA between TATA and Inr showed sensitivity to MPE-Fe, indicating that the DNA helix is not distorted and there are not strong protein-DNA contacts. Therefore, while the DNA needs to bend within this area of the structure, it likely follows a gradual bending path as it enters into lobe A.

1.2 TFIID interacts with diverse promoter architectures through the rearranged conformation

While the SCP DNA has served as an important tool for structurally dissecting the structure of TFIID-TFIIA-SCP, the presence of four consensus promoter motifs in SCP represents a non-physiological arrangement given that most human promoters contain only one or two consensus motifs [5]. To explore the effect of core promoter architecture on TFIID-promoter interactions, DNase I footprinting experiments were performed with mutant SCP DNA constructs in the presence or absence of TFIIA (Figure 1.4). Mutation of the TATA box within the SCP sequence (mTATA) resulted in a wild-type interaction with the promoter DNA from the Inr to the DPE, as seen previously [4]. In addition, the inclusion of TFIIA resulted in a weak but detectable footprint over the mutant TATA box (Figure 1.5). The strong resemblance between the mTATA and the wild-type SCP DNase I protection patterns suggested that TFIID is bound to the mTATA sequence in the rearranged conformation. To test this hypothesis, we collected cryo-EM data and visualized a sample of TFIID-TFIIA-SCP(mTATA) (Figure 1.6). This experiment revealed that TFIID binds to the mTATA promoter in a nearly identical conformation as that observed with the wild-type SCP se-

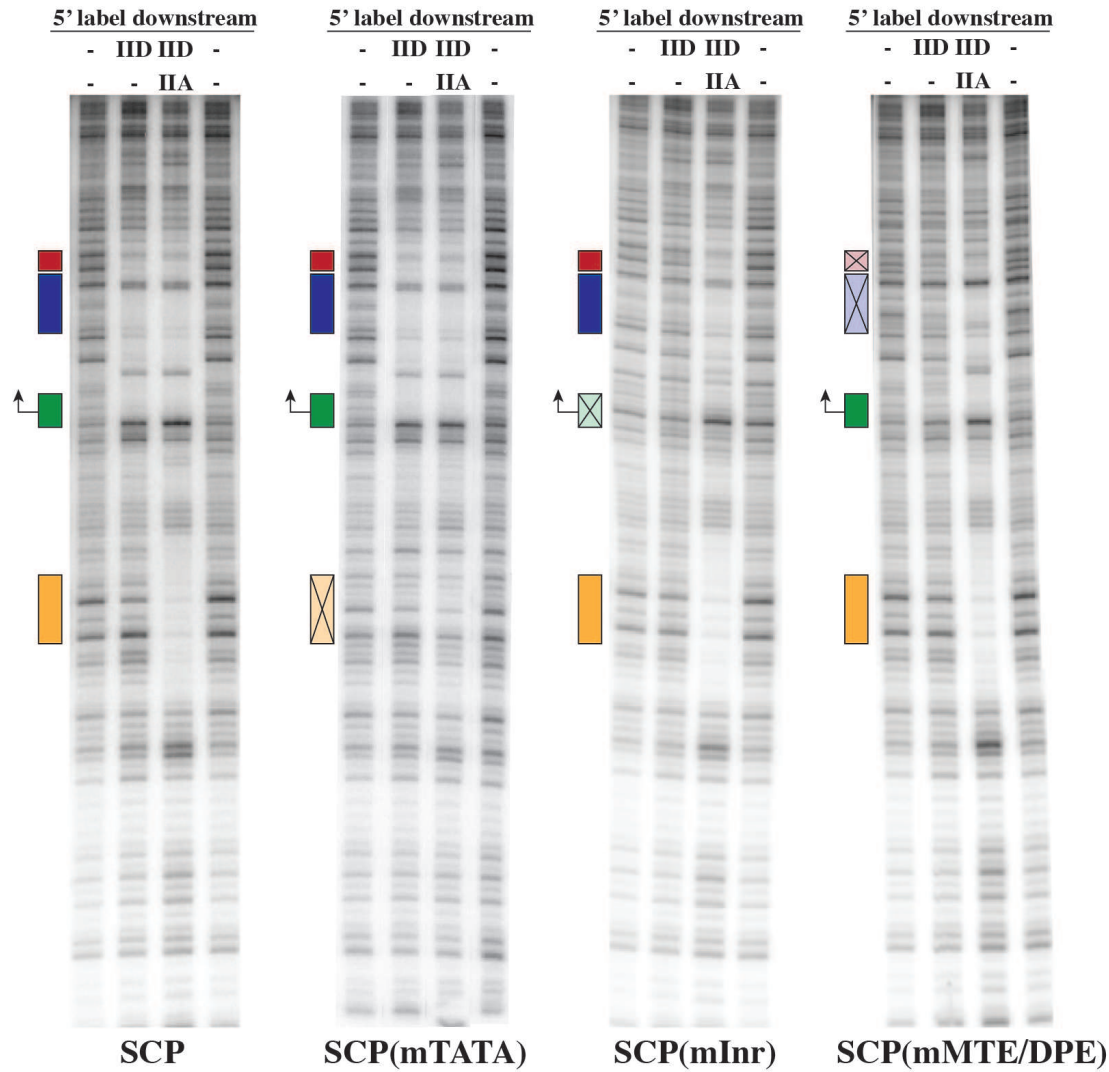


Figure 1.4: Core promoter architecture dictates TFIIA-dependent and TFIIA-independent interactions of TFIID with core promoter DNA. DNase I footprinting on wild type and mutant SCP DNA sequences. 5 labeled downstream probes were analyzed for DNase I protection in the presence or absence of TFIIA for wild type, mutant TATA (mTATA), Inr (mInr), and MTE/DPE (mMTE/DPE).

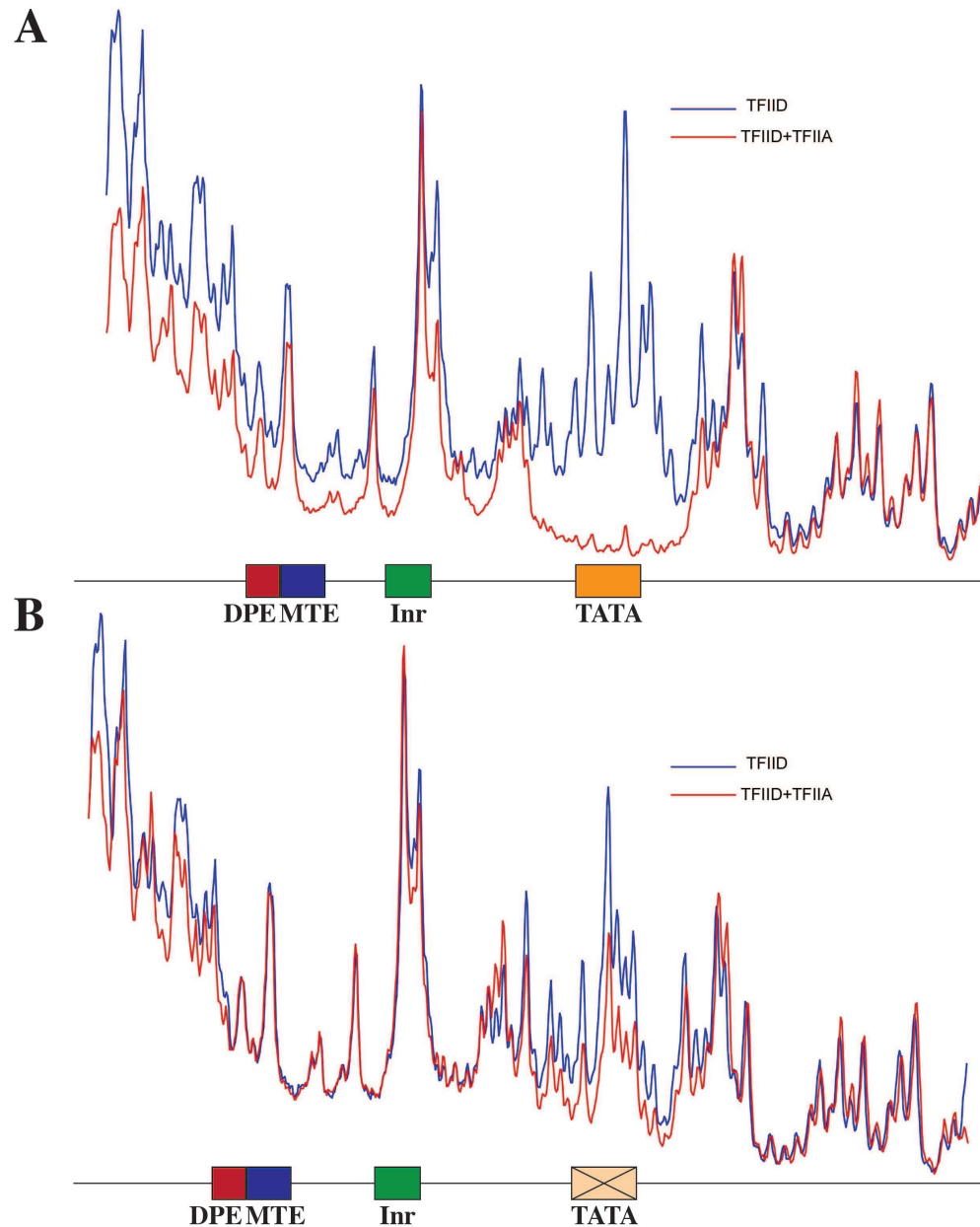


Figure 1.5: Line profiles for DNase I footprinting on mTATA promoter. (A) Line profiles for TFIID (blue) and TFIID-TFIIB (red) on wild-type SCP. (B) Line profiles for TFIID (blue) and TFIID-TFIIB (red) on mTATA promoter.

quence. Thus, the combined footprinting and EM data indicate that the rearranged state of TFIID serves as the predominant DNA binding conformation for the SCP and mTATA promoter architecture.

The conformation of promoter-bound TFIID was further addressed by analysis of promoters that contain mutations in the Inr (mInr) or MTE/DPE (mMTE/DPE) promoter motifs (Figure 1.4). TFIID did not interact appreciably with either the mInr promoter or the mMTE/DPE promoter in the absence of TFIIA, as seen previously [4]. However, the addition of TFIIA resulted in strong binding of TFIID to the TATA box as well as to sequences from the Inr through the DPE regions. In the presence of TFIIA, the overall patterns of protection observed with the mInr and mMTE/DPE promoters are similar to those seen with the wild-type SCP. It thus appears likely that TFIID-TFIIA binds to the mInr and mMTE/DPE promoters in the rearranged conformation. Hence, the footprinting and EM data both suggest that TFIID binds to the wild-type and mutant SCPs in the newly discovered rearranged conformation. With the 'wild-type' SCP as well as with the three 'mutant' (mTATA, mInr, mMTE/DPE) versions of the SCP, we observed that TFIIA stimulates the binding of TFIID to the TATA box region (Figure 1.4). This effect is consistent with the well-established TFIIA-mediated enhancement of TBP binding to the TATA box [11]. With the mTATA promoter, the primary interaction of TFIID with the DNA is via the Inr, MTE, and DPE motifs, and a weak stimulation by TFIIA of the binding of TFIID to the mutant TATA box region is also observed. With the mInr and mMTE/DPE promoters, it seems likely that TFIIA stimulates the binding of TBP to the TATA box and that the remainder of the TFIID complex then interacts with the Inr through the DPE region of the core promoter, irrespective of the presence of consensus Inr or MTE/DPE elements. These findings may be analogous to the previously observed stimulation of the binding of partially-purified TFIID to the downstream promoter region of the adenovirus major late promoter (which lacks MTE/DPE motifs) by the upstream stimulatory factor, USF [10, 15]. In this light, it is possible that other sequence-specific activators, as well as coactivators, may function in a related manner to stabilize TFIID on promoter DNA and thus promote the formation of the rearranged conformation.

1.3 DNA binding within the canonical conformation

While the rearranged conformation is the predominant form of TFIID bound to promoter DNA, we next wanted to investigate if the canonical state is capable of interacting with promoter DNA. Specifically, we wanted to know if the canonical state represented an 'inhibited' structural state of TFIID to bind the MTE/DPE, given the close proximity of lobe A and the MTE/DPE binding sites within the canonical conformation. This investigation into DNA binding by the canonical state is similar in analysis to the localization of TFIIA within lobe A (Figure 1.7A), where 2D reference-free class averages of the canonical were generated and analyzed.

After collecting larger datasets for both +45 and TATA-Nanogold labeled samples, class

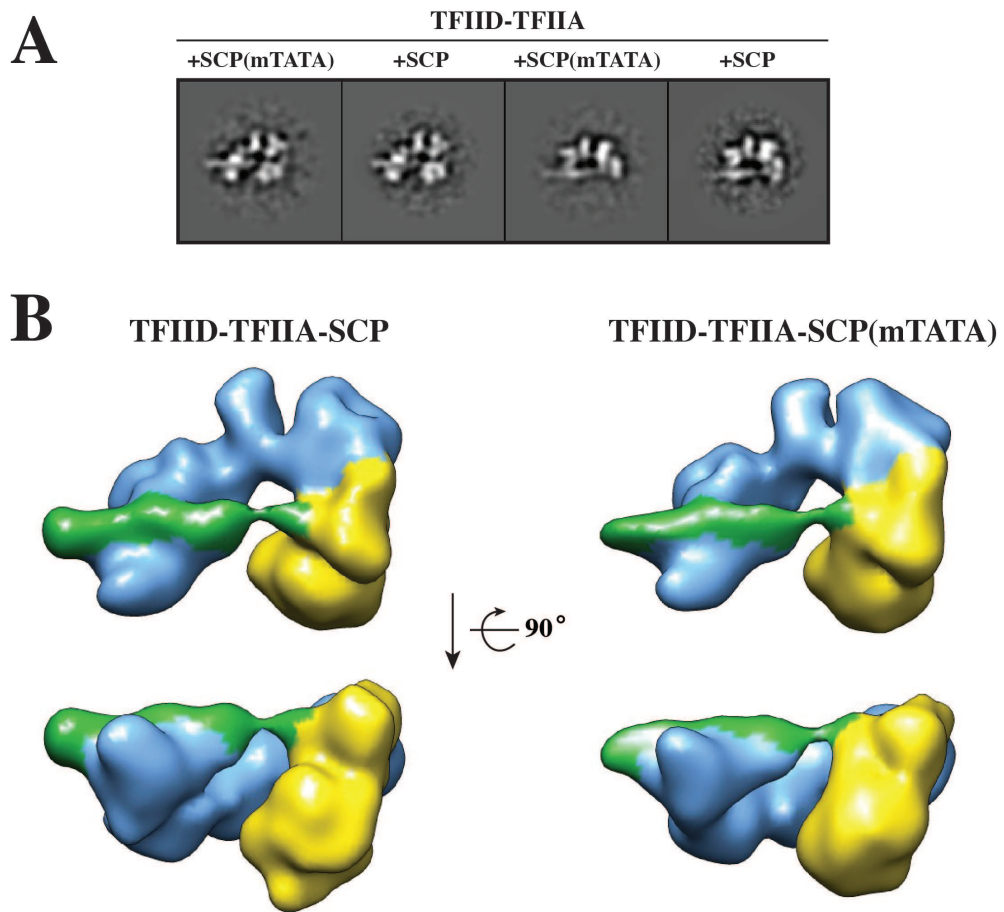


Figure 1.6: TFIID-TFIIA interacts with SCP(mTATA) within the rearranged conformation. (A) 2D reference-free class averages calculated from cryo-EM data of TFIID-TFIIA-SCP(mTATA) are shown alongside 2D reference-free class averages from TFIID-TFIIA-SCP. (B) 3D models of the rearranged conformation for TFIID-TFIIA-SCP and TFIID-TFIIA-SCP(mTATA) at 34 Å.

averages of the canonical conformation for TFIID-TFIIA-SCP showed that the promoter DNA binds in a manner similar to the rearranged conformation. This conclusion comes from comparison of the low defocus thresholded average (Figure 1.7B, right) with the high defocus class averages obtained from alignment and classification (Figure 1.7B, left). The presence of additional density extending away from lobe C in the high defocus average and the terminal localization of +45-Nanogold indicates that SCP DNA is bound. Furthermore, considering the characteristic extension of 15 bps away from lobe C within the rearranged conformation suggests that this additional density extending away from lobe C within the canonical conformation is promoter DNA bound in a near identical manner (Figure 1.7). Unfortunately, the high degree of flexibility of lobe A did not allow careful comparison of lobe A's position and DNA binding, preventing conclusions from being drawn regarding lobe A inhibition of MTE/DPE binding. However, despite this limitation, analysis of the canonical conformation from TFIID-TFIIA-SCP(+45 gold) indicate that the canonical conformation is capable of binding MTE/DPE DNA sequences within the same configuration as the rearranged state.

The binding of MTE/DPE by the canonical suggests that if lobe A engages the TATA box it should occur in a position located away from lobe C. Due to the rigid binding of the MTE/DPE by TFIID within both canonical and rearranged conformations, it is likely that the binding of the TATA box to lobe A occurs in a more flexible manner. To test this, canonical class averages from TFIID-TFIIA-SCP(TATA gold) were analyzed for Nanogold localization (Figure 1.7C). Unlike the stable binding of MTE/DPE to lobe C, the Nanogold signal for TATA gold was diffusey localized along the trajectory of lobe A's rearrangement from making contacts with lobe C (canonical) to lobe B (rearranged). Furthermore, considering the small cluster of peaks at a position opposite the central channel from lobe C, DNA binding in the canonical state positions the TATA box for binding by TBP within lobe A of the rearranged conformation (Figure 1.7C).

Analysis of the highly flexible canonical state using Nanogold labels for TFIIA and DNA has revealed insight into the dynamic process of DNA binding by TFIID (Figure 1.7). While it is difficult to know the position of lobe A within these Nanogold labeled class averages, the Nanogold labeling approach has provided key localizations in an otherwise flexible conformation. Despite the flexibility of lobe A, these labeling data indicate that the canonical conformation is competent for binding to promoter DNA. Lobe C binds to the MTE/DPE sequence in a similar fashion as the rearranged conformation, suggesting that its intrisinc DNA binding activity is preserved within the canonical state. Additionally, as suggested earlier, lobe A appears to exist as a modular TATA binding component of TFIID, where the TATA gold label localized to locations along the path of lobe A's rearrangement.

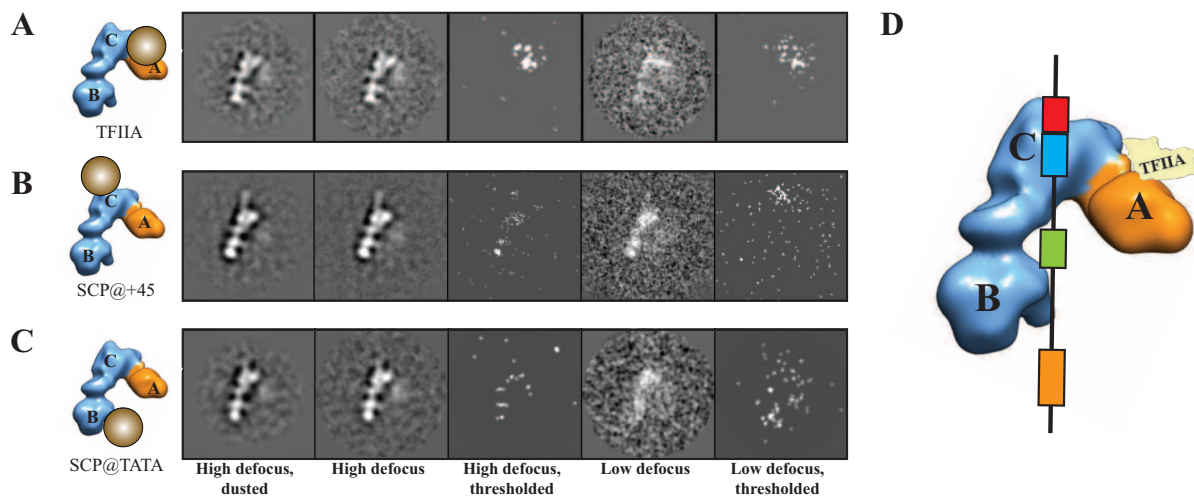


Figure 1.7: Lobe C interacts with promoter DNA within the canonical conformation in a similar manner as the rearranged state. 2D reference-free class averages for the canonical conformation from cryo-EM data of TFIID-TFIIA-SCP with Nanogold labeled TFIIA (A), +45 (B), and TATA (C). Left of the averages is a model of the canonical state indicating location of Nanogold label. (D) Model of DNA path and TFIID within the canonical conformation based upon gold labeling.

1.4 TFIID-TFIIA-TFIIB-SCP adopts the rearranged conformation on promoter DNA

The cryo-EM analysis presented thus far indicates that the predominant DNA binding form of TFIID is the rearranged conformation, suggesting that the remaining general transcription factors may load onto the rearranged state for RNAPII loading. To test this hypothesis, cryo-EM samples were prepared with TFIID-TFIIA-TFIIB-SCP(-66) and analyzed (Figure 1.8). 2D reference-free class averages showed that there were a variety of orientations containing DNA bound to the rearranged conformation (Figure 1.8B). This suggests that the rearranged conformation is the conformation that is bound by TFIIB.

The interaction of TFIIB with TFIID-TFIIA-SCP was further probed through DNase I and MPE-Fe footprinting of reactions containing TFIID, TFIIA, and TFIIB. The footprinting results show that TFIIB extends the length of the footprint previously around the TATA, while the remaining downstream contacts along the Inr, MTE, and DPE remain unchanged (Figure 1.9). Given the bulky nature of DNase I vs. MPE-Fe as footprinting probes, the DNase I footprinting results indicate that an additional 8 - 10 bps are protected on the flanking regions of the TATA box, extending the footprint around the TATA box from -45 to -18 (Figure 1.9A). This shows that nearly 30 bps of promoter DNA upstream of the TSS are sequestered within the TFIID-TFIIA-TFIIB-SCP complex. Furthermore, given that the remaining downstream contacts with promoter DNA are unaffected by TFIIB, these data suggest that TFIIB preferentially interacts with the rearranged conformation. This result is consistent with the labeling of TFIIA and TATA box DNA within lobe A, suggesting that TFIIB binds to promoter DNA within lobe A.

In addition to the DNase I footprinting experiments, MPE-Fe was used in order to provide high-resolution information on the protein-DNA contacts introduced by TFIIB within the TFIID-TFIIA-TFIIB-SCP complex. This analysis revealed that TFIIB makes strong contacts with the flanking DNA sequences around the TATA box from -34 to -19 (Figure 1.9B). These results are consistent with the presence of a downstream BRE motif within the SCP sequence [4], a region of the promoter that is capable of engaging in sequence-specific contacts with TFIIB [1, 12]. Interestingly, however, there are upstream contacts along the upstream BRE motif, even though the SCP sequence does not contain this element [4]. Thus, TFIIB makes specific contacts with the upstream and downstream DNA sequences surrounding the TATA box, potentially stabilizing the TFIID-TFIIA-TFIIB-SCP complex due to an extended footprint on the DNA.

The high affinity binding of TFIID-TFIIA-TFIIB-SCP to the TATA box and flanking sequences suggested that this complex may be able to bind to the mutant TATA sequence within SCP(mTATA). To test this hypothesis, we performed DNase I footprinting of TFIID-TFIIA-TFIIB on wild-type and mutant TATA box promoters (Figure 1.10). The footprinting results revealed that the TATA, upstream BRE, and downstream BRE motifs were no longer strongly protected. Since TFIIB is unable to bind to the upstream and downstream BRE motifs in the absence of TFIIA (Figure 1.9A), the footprinting on SCP(mTATA) suggests

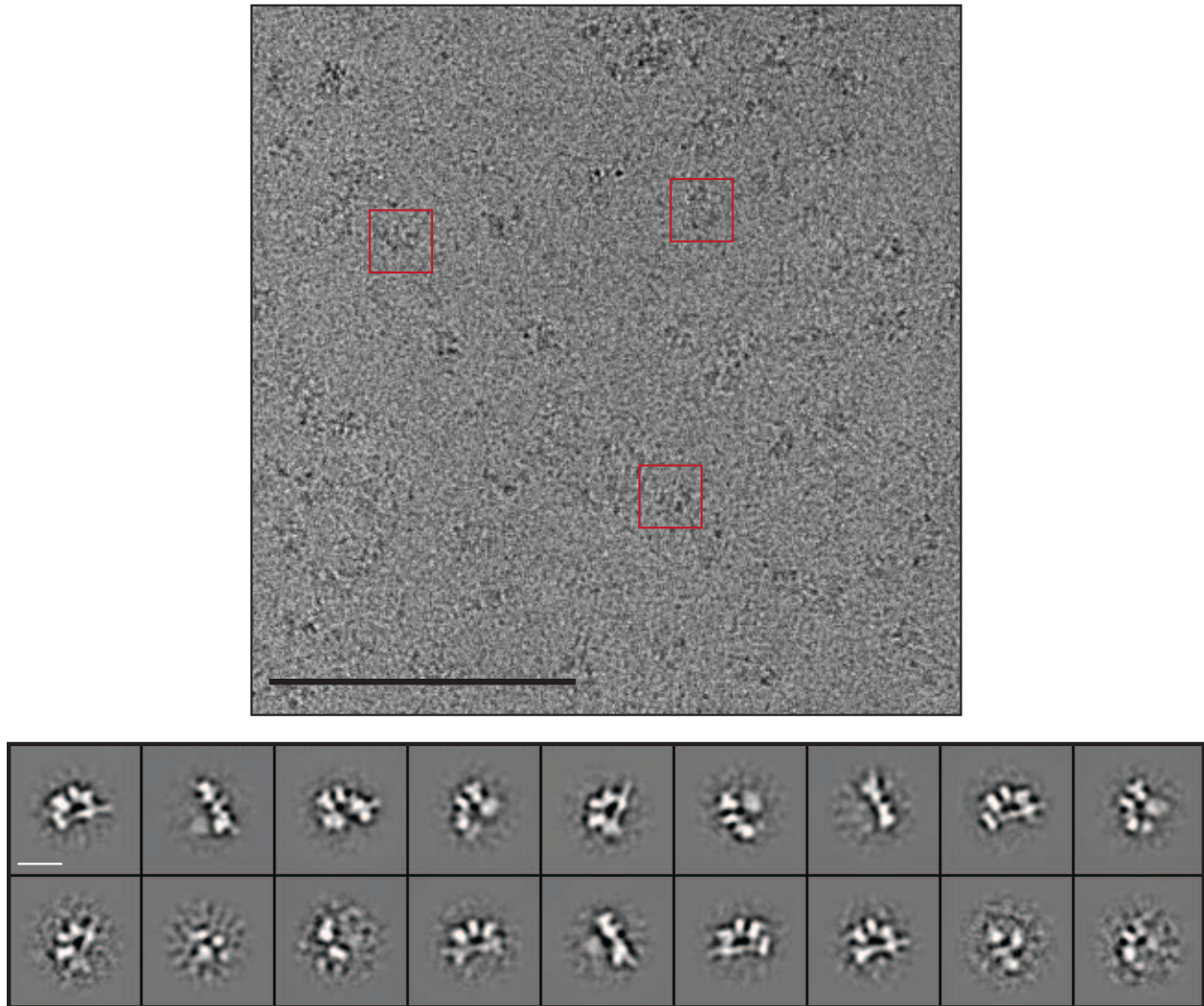


Figure 1.8: Cryo-EM of TFIID-TFIIA-TFIIB-SCP(-66). Representative micrograph (A) and 2D reference-free class averages (B). Scale bar is 200 nm in (A) and 200 Å in (B).

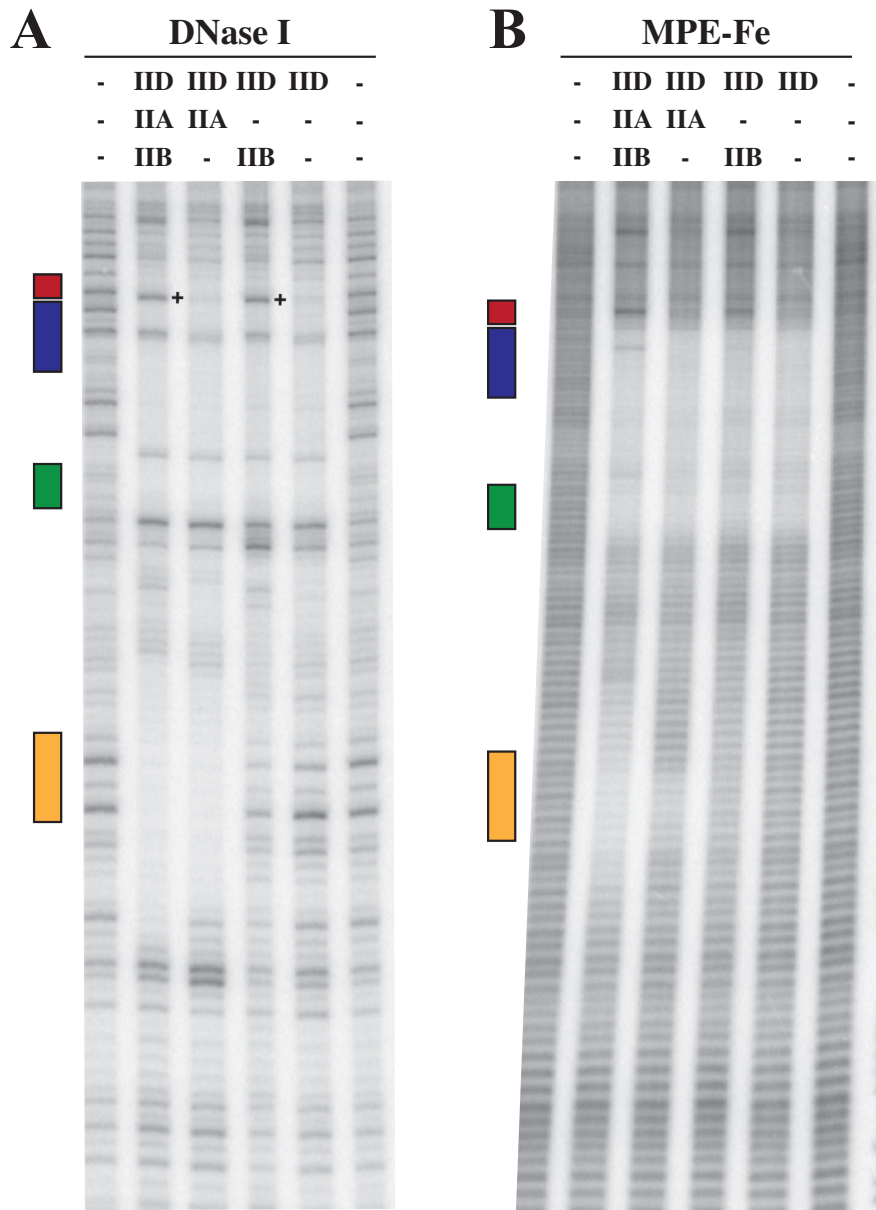


Figure 1.9: TFIIB interacts with TFIID-TFIIA-SCP within the rearranged conformation on promoter DNA. DNase I (A) and MPE-Fe (B) footprinting of TFIID-TFIIA-TFIIB-SCP on 5'-labeled downstream DNA.

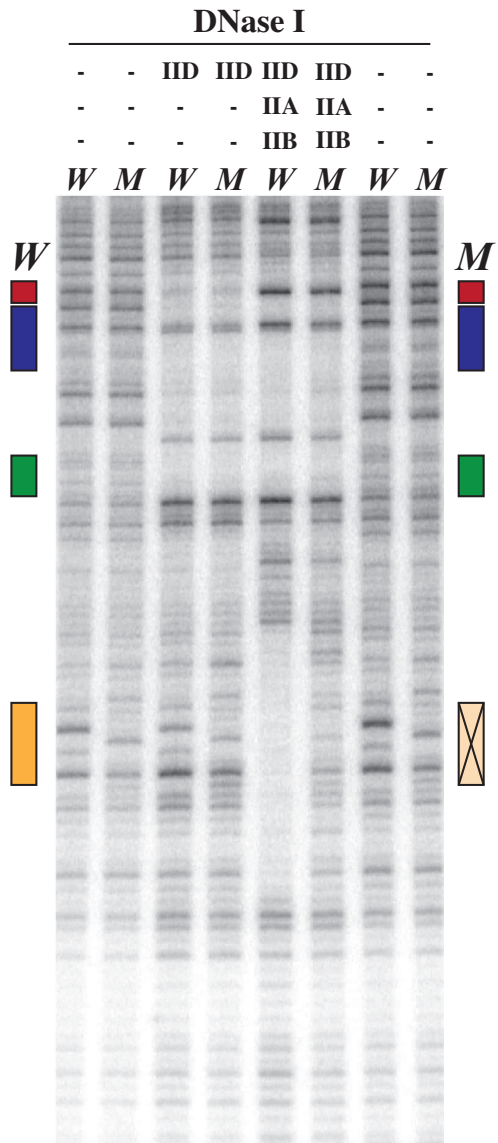


Figure 1.10: TFIIB does not induce strong TATA box protection within TFIID-TFIIA-TFIIB-SCP(mTATA). DNase I footprinting of TFIID-TFIIA-TFIIB on SCP(mTATA). *W* and *M* indicate wild-type SCP and SCP(mTATA) promoters, respectively.

a cooperative activity of TFIIB-TBP-TATA in order for high affinity binding to the TATA, upstream BRE and downstream BRE motifs. This explanation is consistent with the crystal structure of TBP-TFIIB-TATA, where the TFIIB simultaneously contacts TBP, upstream BRE, and downstream BRE [12]. It should be noted, however, that there is slight protection of the TATA sequence, comparable to that previously observed (Figure 1.5), indicating that TBP may be within close proximity of the mutated TATA sequence. These footprinting data suggest that, within the context of a mutant TATA box, TFIIB does not stimulate DNA binding by TBP nor does it interact with the downstream BRE element, suggesting that TFIIB may be binding to the TFIID-TFIIA-SCP(mTATA) complex.

The data above indicate that TFIIB binds the rearranged conformation in the presence of a functional TATA box and, given the extended footprinting surrounding the TATA box, the binding of TFIIB to TFIID-TFIIA-SCP may stabilize the ternary complex to enable high resolution studies. Therefore, 3D refinements were performed on a sample of TFIID-TFIIA-TFIIB-SCP(-66) using previously obtained models corresponding to the canonical and rearranged conformations. After collecting and analyzing 56,000 cryo-EM particles of TFIID-TFIIA-TFIIB-SCP, the resulting 3D refined model for the rearranged state achieved a resolution of 36Å, comparable to that obtained previously for TFIID-TFIIA-SCP. To investigate if the binding of TFIIB to the ternary complex altered structural contacts between components within TFIID-TFIIA-SCP, the structure is shown alongside the previously obtained TFIID-TFIIA-SCP(-66) (Figure 1.11). The overall structural features of these two models are nearly the same at this resolution, indicating that TFIIB does not introduce global changes in the structure of TFIID-TFIIA-SCP upon binding.

Despite these similarities, there are subtle changes of the DNA density within the TFIID-TFIIA-TFIIB-SCP(-66) structure. First, as a positive control, this sample was prepared with SCP(-66) to test the presence and location of the upstream DNA density that was identified previously (Figure ??). Since the initial 3D model used for refinement did *not* contain density corresponding to the upstream DNA, the presence of additional density exiting lobe A in a near-identical location suggests that position of upstream DNA does not change relative to the TATA box within TFIID-TFIIA-TFIIB-SCP(-66) (Figure 1.11). Interestingly, however, the shape of the DNA density appears to be narrower than the previously determined structure. This may be due to the increased rigidity of upstream DNA because of the TFIIB-mediated contacts along the flanking DNA sequences around the TATA box (Figure 1.9A). Despite visualizing this change in upstream DNA, we were unable to detect any differences within lobe A (or any part of the TFIID structure) that is consistent in size with TFIIB (30 kDa). For clarity, the previously proposed atomic model of promoter DNA, TBP, TFIIA, and TFIIB were docked into the TFIID-TFIIA-TFIIB-SCP(-66) structure, which shows that the area of the proposed TFIIB binding site appears very similar between both structures. While TFIIB likely interacts with the rearranged conformation, the low resolution of the model prevents further conclusions to be drawn regarding an structural consequences of TFIIB binding.

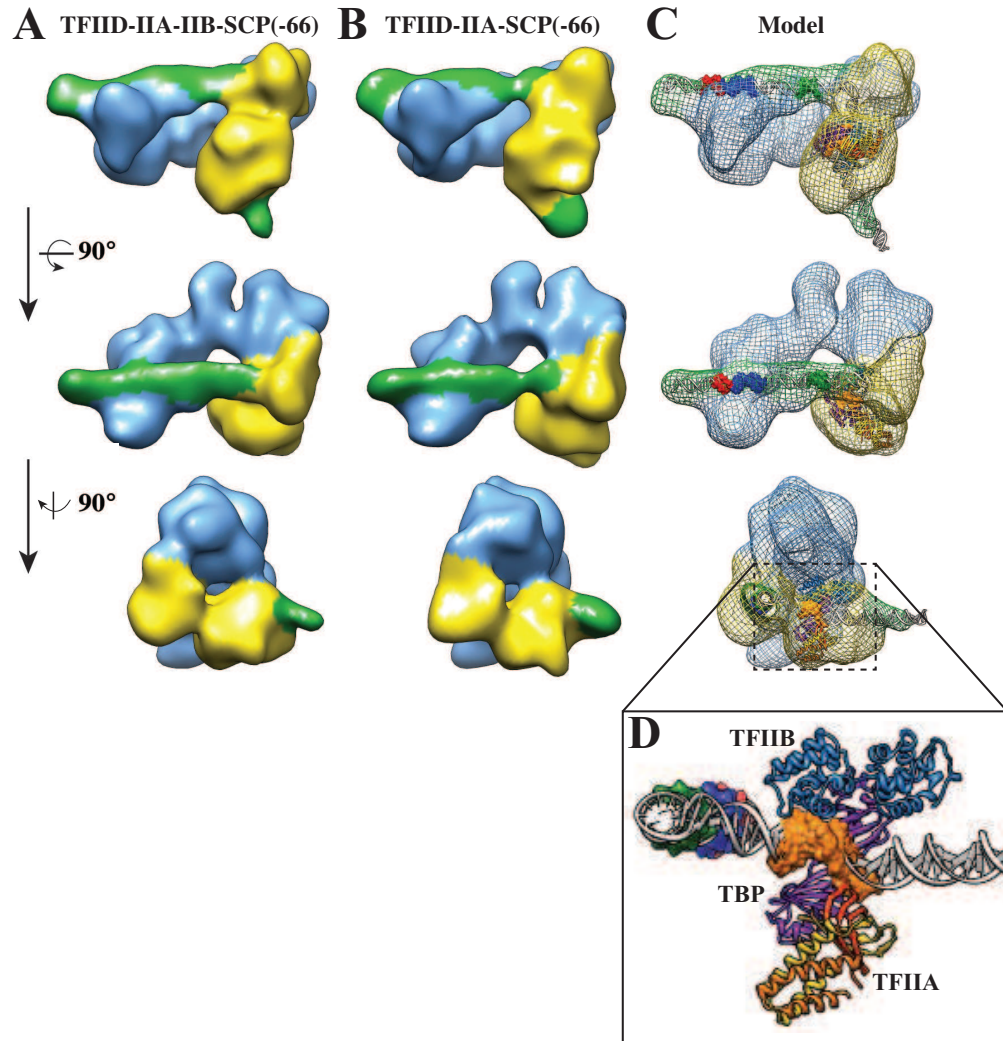


Figure 1.11: 3D reconstruction of the rearranged conformation of TFIID-TFIIA-TFIIB-SCP(-66) reveals similar topology as TFIID-TFIIA-SCP(-66). 3D models for rearranged conformation of TFIID-TFIIA-TFIIB-SCP(-66) (A) and TFIID-TFIIA-SCP (B) at 36 Å. (C) Docked DNA model for -66 to +45 with TBP-TFIIB-TFIIA crystal structure model (D) from Figure ??

1.5 A general model of regulated DNA binding by TFIID

The structural work presented within this chapter has served to test and extend a model for promoter binding by TFIID. In order to model TFIID's interaction with promoter DNA, the model must take into account the interplay between TFIID's conformational dynamics and promoter binding. Therefore, the following models have been proposed in an attempt to summarize the structural data presented throughout Chapters 2, 3 & 4 (Figures 1.12 - 1.14). While the rearranged state likely serves as the predominant high affinity DNA binding conformation of TFIID, the structural data presented here present alternative structural pathways for TFIID interacting with promoter DNA. Even though all of the experiments presented here were performed under equilibrium conditions, we believe that the equilibrium experiments implicitly inform us on the directionality of this structural path taken by TFIID. The models that we proposed dependent on the interplay between core promoter architecture and TFIIA and, therefore, our models have been separated into based upon the core promoter architecture: SCP (Figure 1.12), SCP(mTATA) (Figure ??), and SCP(mMTE/DPE) (Figure 1.14). Broadly, we believe these models serve as a framework for understanding TFIID's pleiotropic interactions with promoter DNA in an activator-dependent manner.

TFIID-TFIIA-SCP

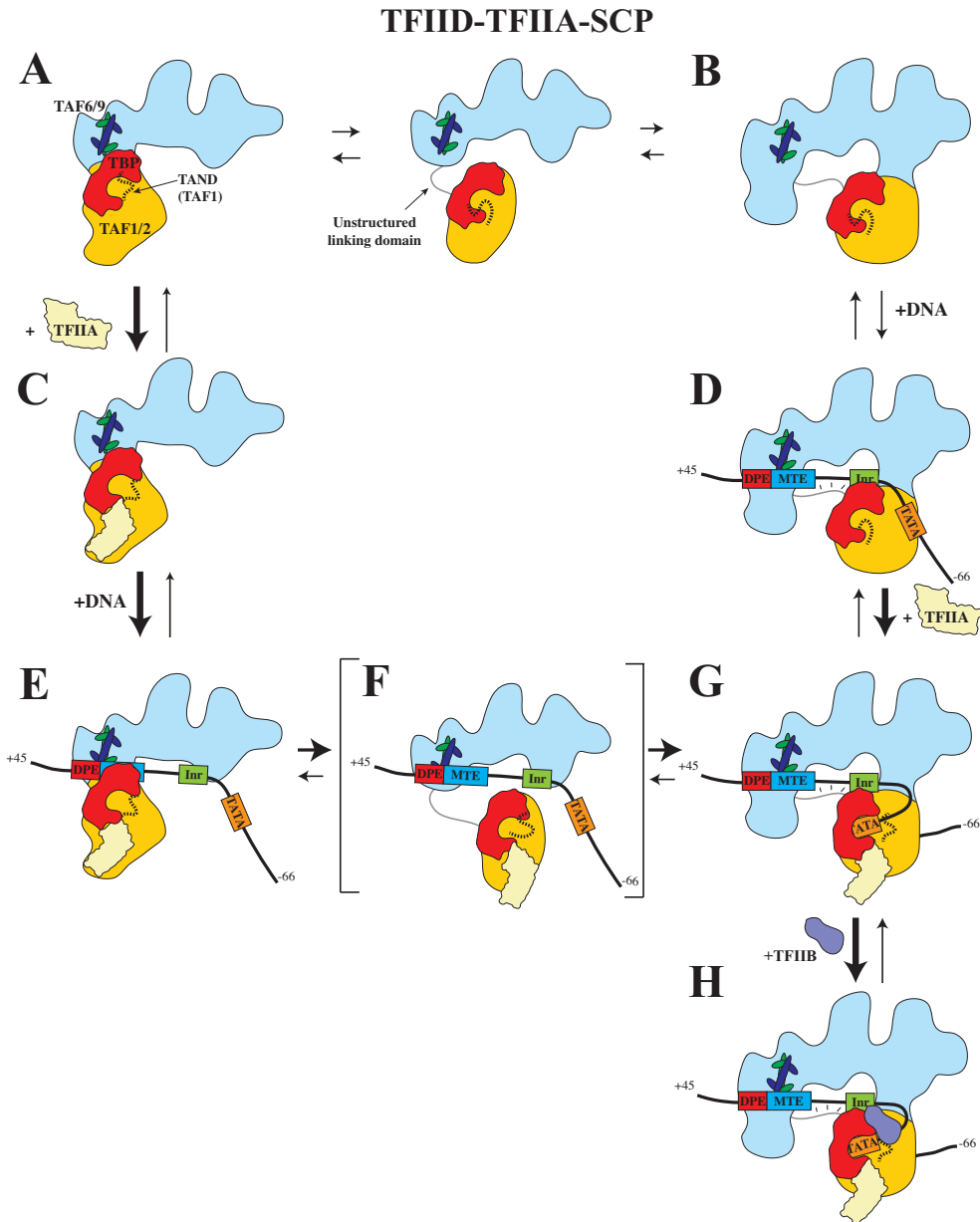


Figure 1.12: Model for SCP DNA binding by TFIID-TFIIA. TFIID undergoes conformational changes between canonical (A) and rearranged (B) states. The addition of TFIIA stabilizes the canonical conformation (C). Alternatively, the addition of SCP DNA leads to binding of the Inr-MTE/DPE to the rearranged conformation (D). The combined presence of TFIIA and SCP DNA leads to a stabilization of the rearranged conformation (G). While most particles adopt the rearranged state for TFIID-TFIIA-SCP, there is a small subset that is bound to SCP DNA and TFIIA within the canonical state (E). This state converts to the rearranged state through a likely intermediate state (F). The rearranged TFIID-TFIIA-SCP conformation can then be bound by TFIIB to load RNAPII.

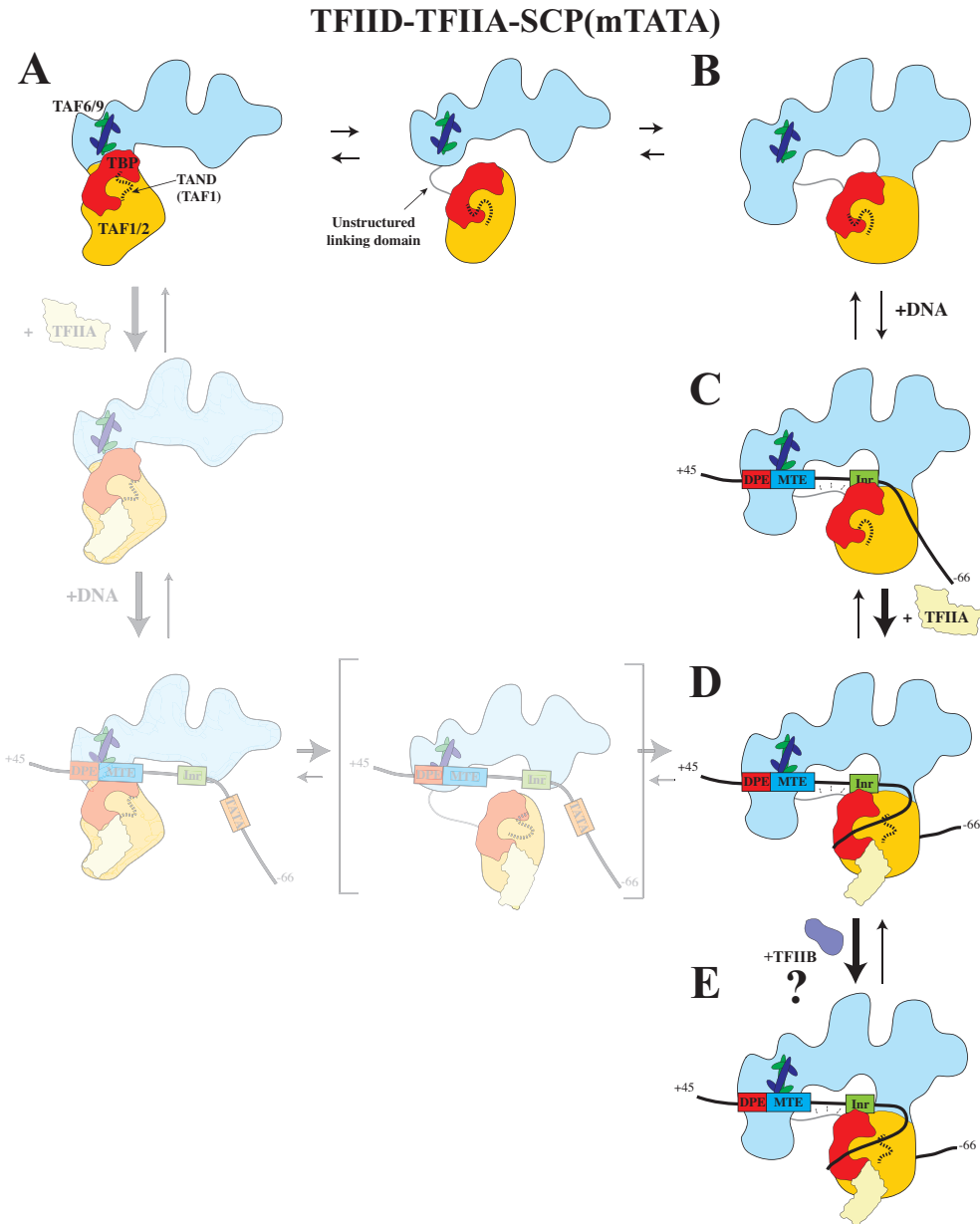


Figure 1.13: Model for SCP(mTATA) DNA binding by TFIID-TFIIA. TFIID undergoes conformational changes between canonical (A) and rearranged (B) states. The addition of SCP(mTATA) interacts with the rearranged conformation (C) that is further stabilized by TFIIA (D). Note that the DNA likely makes weak contacts with the surface of TFIID near TBP without TBP engagement of DNA. The rearranged TFIID-TFIIA-SCP(mTATA) conformation should then be bound by TFIIB, although it is difficult to know where within the TFIID structure it will bind (E).

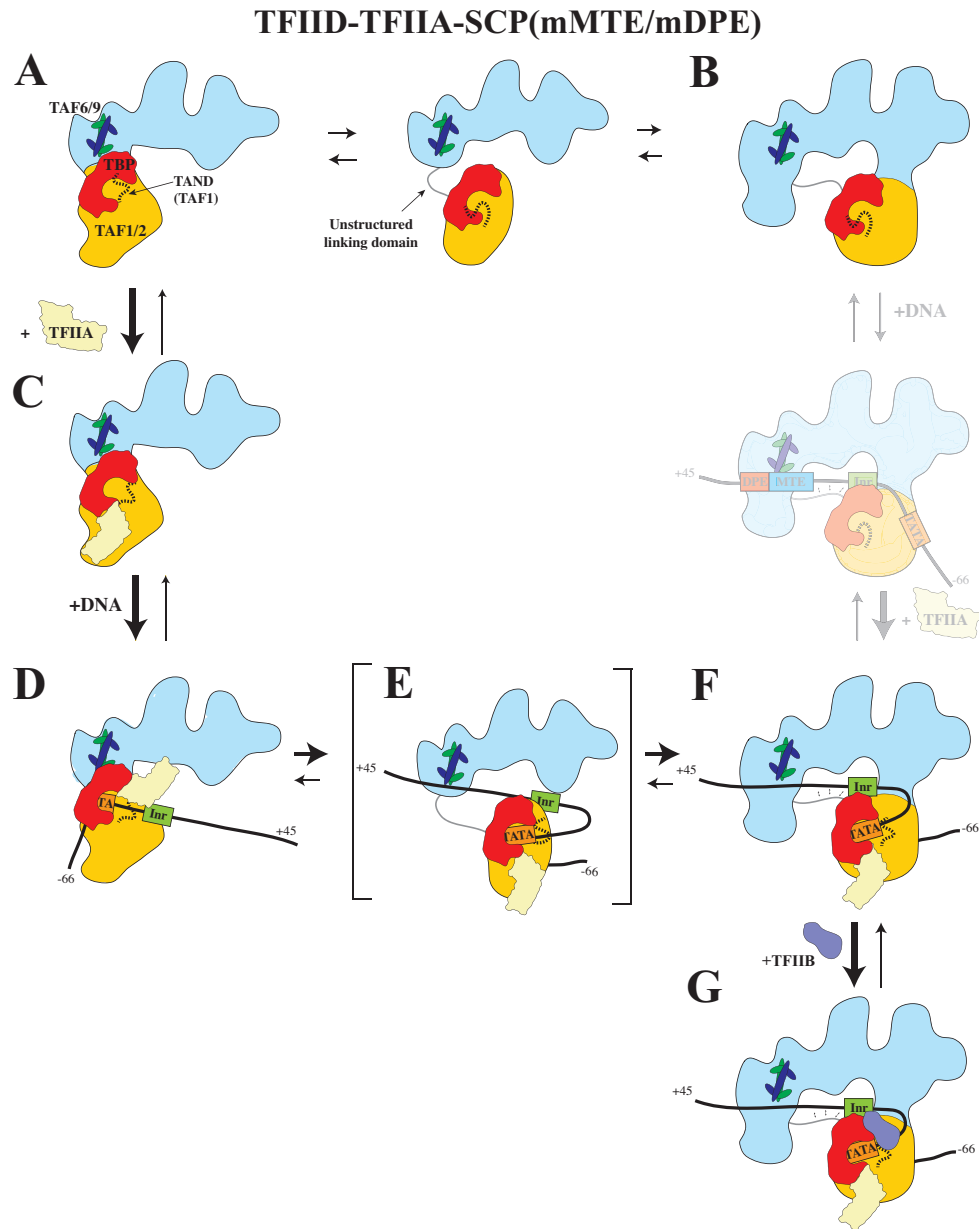


Figure 1.14: Model for SCP(mMTE/DPE) DNA binding by TFIID-TFIIA. TFIID undergoes conformational changes between canonical (A) and rearranged (B) states. The addition of TFIIA stabilizes the canonical conformation (C). The addition of SCP(mMPE/DPE) leads to the formation of the rearranged conformation (F) through the proposed intermediates of (D) and (E). The rearranged TFIID-TFIIA-SCP(mMTE/DPE) conformation can then be bound by TFIIB to load RNAPII (G).

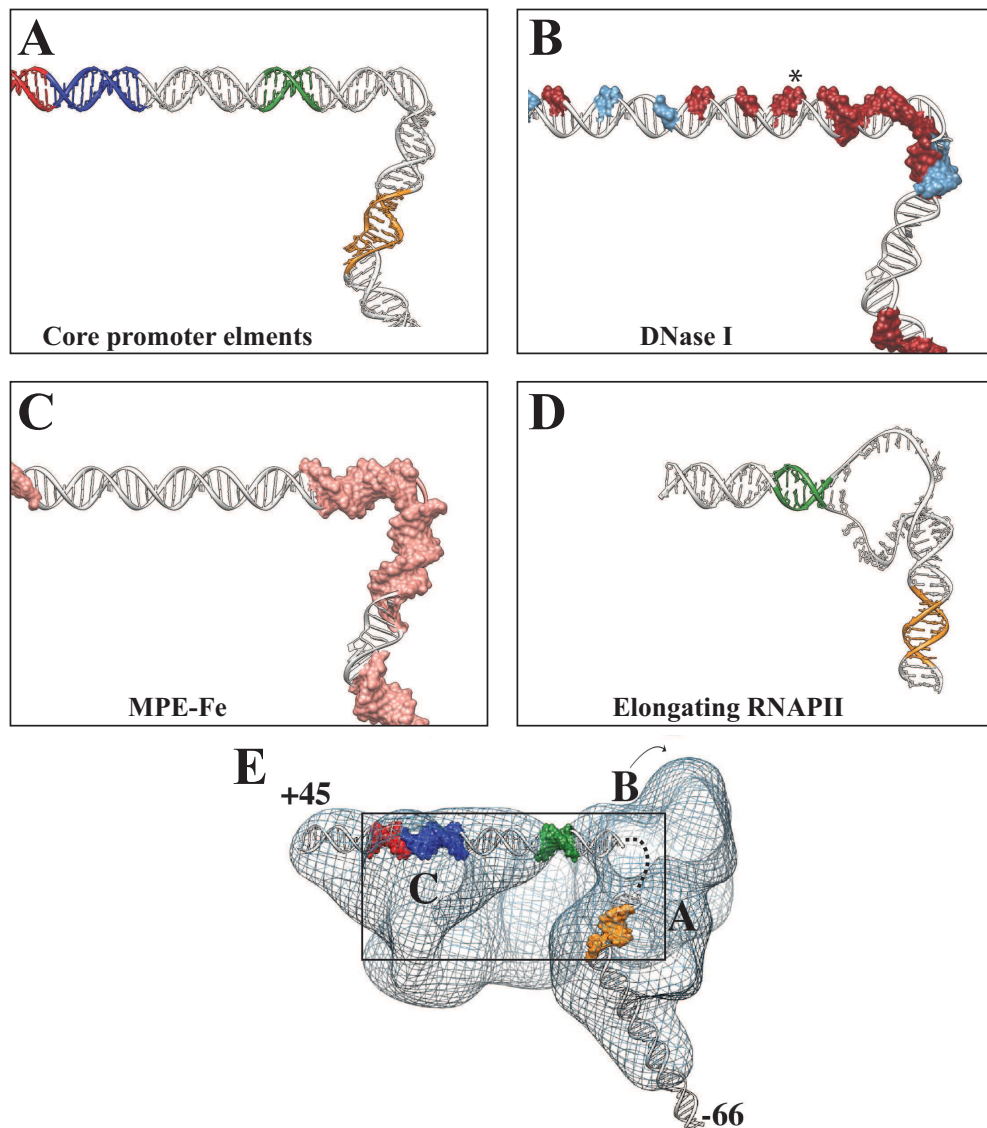


Figure 1.15: TFIID may facilitate transcription initiation through topological changes in promoter DNA. Model of promoter DNA path through TFIID-TFIIA-SCP(-66) for core promoter element location (A), DNase I footprinting (B), and MPE-Fe footprinting (C). Shown alongside the modeled DNA path through an elongating RNAPII (adopted from PDB 3PO3). (E) Corresponding view from TFIID-TFIIA-SCP(-66) model.

Chapter 2

Conclusions and outlook

Future directions for TFIID research

Appendix A

methods

Bibliography

- [1] W. Deng and S. G. Roberts. “A core promoter element downstream of the TATA box that is recognized by TFIIB”. In: *Genes Dev* 19.20 (2005), pp. 2418–23.
- [2] J. H. Geiger et al. “Crystal structure of the yeast TFIIA/TBP/DNA complex”. In: *Science* 272.5263 (1996), pp. 830–6.
- [3] R. P. Hertzberg and P. B. Dervan. “Cleavage of DNA with methidiumpropyl-EDTA-iron(II): reaction conditions and product analyses”. In: *Biochemistry* 23.17 (1984), pp. 3934–45.
- [4] T. Juven-Gershon, S. Cheng, and J. T. Kadonaga. “Rational design of a super core promoter that enhances gene expression”. In: *Nat Methods* 3.11 (2006), pp. 917–22.
- [5] T. Juven-Gershon and J. T. Kadonaga. “Regulation of gene expression via the core promoter and the basal transcriptional machinery”. In: *Dev Biol* 339.2 (2010), pp. 225–9.
- [6] J. L. Kim, D. B. Nikolov, and S. K. Burley. “Co-crystal structure of TBP recognizing the minor groove of a TATA element”. In: *Nature* 365.6446 (1993), pp. 520–7.
- [7] Y. Kim et al. “Crystal structure of a yeast TBP/TATA-box complex”. In: *Nature* 365.6446 (1993), pp. 512–20.
- [8] D. B. Nikolov et al. “Crystal structure of a TFIIB-TBP-TATA-element ternary complex”. In: *Nature* 377.6545 (1995), pp. 119–28.
- [9] A. G. Papavassiliou. “Chemical nucleases as probes for studying DNA-protein interactions”. In: *Biochem J* 305 (Pt 2) (1995), pp. 345–57.
- [10] M. Sawadogo and R. G. Roeder. “Interaction of a gene-specific transcription factor with the adenovirus major late promoter upstream of the TATA box region”. In: *Cell* 43.1 (1985), pp. 165–75.
- [11] M. C. Thomas and C. M. Chiang. “The general transcription machinery and general cofactors”. In: *Crit Rev Biochem Mol Biol* 41.3 (2006), pp. 105–78.
- [12] F. T. Tsai and P. B. Sigler. “Structural basis of preinitiation complex assembly on human pol II promoters”. In: *EMBO J* 19.1 (2000), pp. 25–36.
- [13] K. Uchida et al. “High resolution footprinting of EcoRI and distamycin with Rh(phi)2(bpy)3+, a new photofootprinting reagent”. In: *Nucleic Acids Res* 17.24 (1989), pp. 10259–79.

- [14] M. W. Van Dyke, R. P. Hertzberg, and P. B. Dervan. “Map of distamycin, netropsin, and actinomycin binding sites on heterogeneous DNA: DNA cleavage-inhibition patterns with methidiumpropyl-EDTA.Fe(II)”. In: *Proc Natl Acad Sci U S A* 79.18 (1982), pp. 5470–4.
- [15] M. W. Van Dyke, R. G. Roeder, and M. Sawadogo. “Physical analysis of transcription preinitiation complex assembly on a class II gene promoter”. In: *Science* 241.4871 (1988), pp. 1335–8.